August 2003. One patient who had 3 pial AVMs was included, and thus 28 AVMs were used for evaluation. The median age of the patients was 51 years and ranged from 13 to 69 years. There were 16 male and 10 female patients. The 28 AVMs included five infratentorial lesions, with the rest being located at the cerebrum. Conventional stereotactic biplanar digital subtracted angiography (DSA) (Advantx LCN; GE, Milwaukee, WI) was conducted on all patients by immobilizing them using a stereotactic frame with fiducial markers attached at the front, back, and sides of the frame. The targets were delineated by a neuroradiologist. The coordinates of the center of the nidus and the maximum diameter were calculated using software based on the calculation method proposed by Shidon and Barth (13). The MRA was obtained on a 1.5-Tesla MR scanner with a standard head coil (Magnetom Symphony; Siemens, Erlangen, Germany) on all patients 3–5 days before treatment planning. Three-dimensional time-of-flight MRA was performed after the injection of 0.2 mL of gadodiamide per kilogram of body weight. The imaging parameters were as follows: TR = 37 ms, TE = 7.15 ms, flip angle = 25°, band width = 100 Hz per pixel, section thickness = 0.5 mm, field of view = 150 × 200 mm, matrix = 230 × 512, partitions = 60, 3 slabs, acquisition time = 9 min 39 s. The total number of sections was 138. The resultant voxel dimensions were 0.9 × 0.4 × 0.5 mm. Magnetization transfer was used. The acquisition volume was placed in an oblique axial direction so that the volume included the whole of the AVM. Computed tomography (CT) for radiation treatment planning (plan-CT) was performed on all patients, with the patient immobilized by the same stereotactic frame by the CT machine (Sfida, SCT-7000TX/TH; Shimazu, Kyoto, Japan), with a slice thickness of 3 or 5 mm and a matrix size of 256 × 256 with a field of view of 280 mm. The source date of the MRA was three-dimensionally coregistered to the plan-CT based on 6–10 anatomic landmarks on a commercially available registration machine, which has been described elsewhere (14). The nidus of the AVM was delineated on the MRA coregistered with the plan-CT (Fig. 1) by radiation oncologists first. Neuroradiologists and neurosurgeons modified the target if necessary. The center and maximum diameter of the nidus were used for this analysis.

In 15 of the 28 AVMs, CTA was performed immediately after stereotactic DSA. A scanner capable of spiral data acquisition with an injection of contrast medium was used (GE IVR Angio CT System, Advantx ACT [Advantx LCN, HiSpeed LX/I]; GE, Milwaukee, WI). The contrast medium was given via an intravascular catheter placed in the proximal arteries of the AVMs. The CTA protocol consisted of conventional unenhanced scanning with 5–10-mm slice thickness, followed by helical scanning during rapid injection of contrast medium, and finally conventional delayed postcontrast scanning with 5–10-mm slice thickness. Helical scanning was performed using 3× diluted contrast medium at a rate of 2.5 mL/s with a prescan delay time determined by the information from the stereotactic DSA. The CTA data were transferred as MRA to plan-CT. The delineation made by the MRA was modified using the CTA data in these 15 patients. The role of the additional information of CTA to MRA was evaluated.

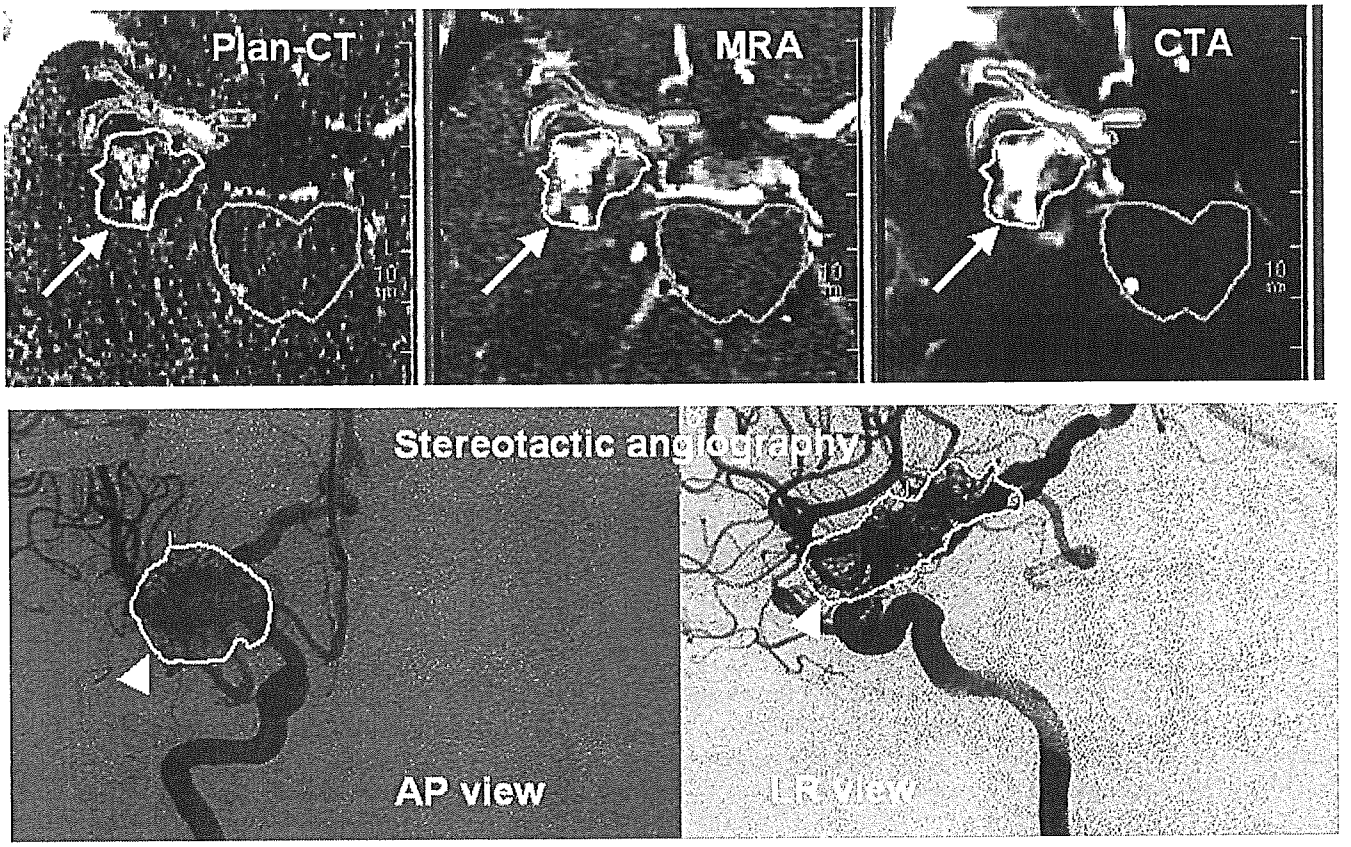

Fig. 1. A case in which the arteriovenous malformation (AVM) target was delineated on coregistered contrast-enhanced computed tomography (CT), contrast-enhanced magnetic resonance angiography (MRA), and computed tomographic angiography (CTA) (arrow). Target on AP and LR view of stereotactic angiography are also shown (arrowhead). AP = anterior-posterior; LR = left-right.

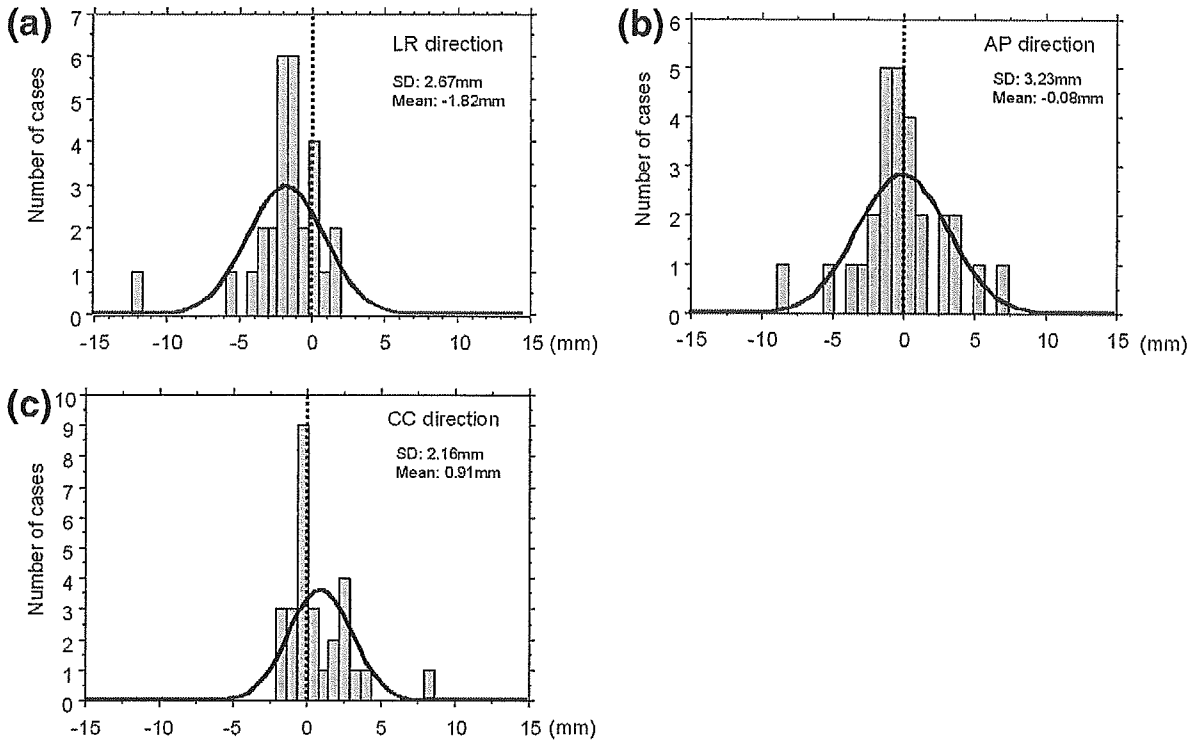

Fig. 2. Distributions of the displacement of centers between magnetic resonance angiography (MRA)-based arteriovenous malformation (AVM) and angiography-based AVM in (a) left-right (LR) direction, (b) anterior-posterior (AP) direction, and (c) craniocaudal (CC) direction.

The discrepancies between the target on conventional stereotactic DSA (V_{DSA}) and the target on the MRA (V_{MRA}) in the coordinates of the center of the nidus, the maximum diameter, and the volume of the nidus assuming an ellipsoidal shape were measured. The coordinates of the outer edge of the nidus were also measured. If V_{MRA} alone is used to determine the target volume, it may not cover V_{DSA}. This issue was addressed in each dimension by calculating the ratio of the maximum length of the intersection of the V_{MRA} with the V_{DSA} to the maximum length of the V_{DSA} in that dimension. This calculation was repeated in all three orthogonal dimensions.

RESULTS

Displacement of the centers of targets between V_{DSA} and V_{MRA}

The standard deviation (mean value) of the displacement of the center of V_{MRA} to the center of V_{DSA} was 2.67 mm (−1.82 mm) in the left-right (LR) direction, 3.23 mm (−0.08 mm) in the anterior-posterior (AP) direction, and 2.16 mm (0.91 mm) in the craniocaudal (CC) direction (Figs. 2a, 2b, 2c). The root-mean-square displacement, an estimation of 3D distance, was 4.7 ± 2.9 mm. There were 2 AVMs (7%) for which the 3D displacement was 1 cm or more, 6 AVMs (21%) with a distance ranging from 5 mm to 1 cm, 12 AVMs (43%) with distances from 2 mm to 5 mm, and 8 AVMs (29%) of 2 mm or less. No correlation between the size of the nidus and degree of displacement was found (Fig. 3). Retrospective analysis suggested that the displacement of centers over 1 cm was attributed to the low quality of conventional stereotactic DSA as a result of the overlapping of major vessels in 1 case (AVM-12) and the poor depiction of the MRA in 1 case (AVM-23).

Size and volume assessment

The mean maximum diameter of V_{DSA} in the LR, AP, and CC directions was 2.206 cm, 2.369 cm, and 2.106 cm,

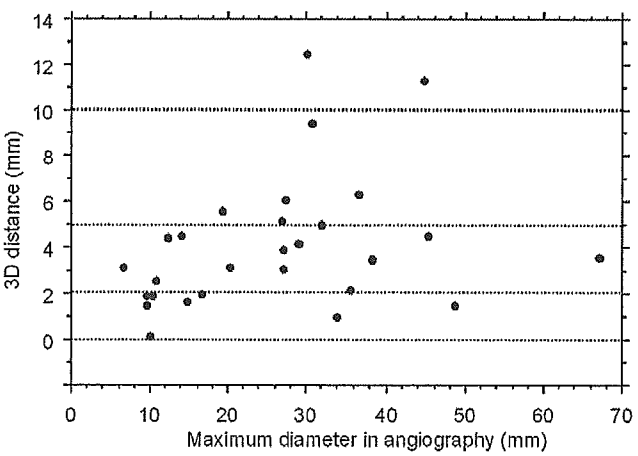

Fig. 3. Three-dimensional displacement of magnetic resonance angiography (MRA)-based arteriovenous malformations (AVMs) from angiography-based AVMs in relation to the maximum diameter of the AVMs.

respectively. These values of V_{MRA} were 2.287 cm, 2.632 cm, and 2.138 cm, respectively. The difference was not statistically significant in all directions, with p values of 0.797 for the LR direction, 0.502 for the AP direction, and 0.928 for the CC direction. The average nidus volume of V_{DSA} was 11.9 cc (range, 0.1–118.1 cc); for V_{MRA}, it was 12.3 cc (range, 0.20–97.2 cc). The difference was not statistically significant by Student's t-test analysis (p = 0.948).

The coverage of V_{DSA} by V_{MRA}

The mean percent coverage of V_{DSA} by V_{MRA} was 88.9% (range, 33–100%) in the LR direction, 90.9% (range, 61.0–100%) in the AP direction, and 91.0% (range, 64–100%) in the CC direction. There were nine AVMs for which the coverage ratio was less than 80% in any direction (Table 1). The low coverage of these nine AVMs was considered to be attributed to the underestimation by V_{MRA} in eight AVMs, and the overestimation on angiography in 1 patient in the retrospective assessment.

The impact of the use of CTA in addition to MRA

The clarity of visualization of the AVMs was rated for the CTA and MRA separately by a single investigator (H.A.). These images were rated "clear" if abnormal vascular structures were easily identified and "unclear" if the abnormal vascular structure was vague and difficult to identify. AVM on CTA was rated "clear" in 13 cases (87%), whereas that on MRA was rated "clear" in 10 cases (67%)(χ square, p = 0.38). In cases in which the visualization of AVM on the MRA was "unclear," the targets were delineated based on the information provided by either the CTA or plan-CT as a platform of dose calculation. Statistically significant improvement was not observed with regard to the displacement of centers between the V_{MRA} delineated on MRA alone and that on CTA in addition to MRA (Table 2). However, the CTA gave us useful flow dynamics–related information in the case of a relatively large AVM (AVM-22), and we omitted the portion of the draining vein from the target (Fig. 4).

DISCUSSION

In the radiosurgical treatment planning of intracranial AVM, the importance of the integration of 3D-image information on stereotactic angiography has been widely recognized since the 1990s. MRA and CTA have both been investigated for this purpose. Bednarz *et al.* combined contrast-enhanced time-of-flight MRA and stereotactic angiography in the treatment planning of 22 AVMs (3). They found that the treatment plans were modified in 12 patients (55%) after inclusion of the MRA data. Kondziolka *et al.* used MRA for radiosurgical treatment and found that the MRA provided additional critical information on the shape of the AVM in 16 of 28 (57%) patients (4). They suggested the possibility of doing treatment planning with MRA without conventional angiography. In our study, we discovered that the displacement of centers between V_{MRA} and V_{DSA} was greater than 5 mm in one-third of the cases, regardless of the size of the AVMs, a fact that has not been well documented in previous publications. In addition, no significant difference was seen between the measurements of V_{MRA} and those of V_{DSA}. However, the MRA-based target did not adequately cover the angiography-based target in one-third of the cases. Although it is difficult to judge which is more accurate, because pathologic confirmation of the real shape of the AVM is impractical, the results of this study suggest that the use of MRA alone for the target delineation might lead to missing some of the target volumes and could result in compromised treatment outcomes.

Tanaka *et al.* evaluated the conspicuity of the nidus by MRA and CTA (12). They found that MRA failed to discriminate 21 (68%) of 31 draining veins that were detected by angiography and that CTA failed to discriminate 12 (50%) of 24 feeding arteries. On the other hand, MRA successfully discriminated 19 (79%) of 26 feeding arteries, and the CTA depicted 18 (78%) of 23 draining veins, but it was not certain whether MRA and CTA could work complementarily to detect the accurate shape of nidus. We addressed this concern by comparing target delineated on MRA alone and target done on CTA in addition to MRA in regard to the discrepancy of centers; however, the results did not suggest that the complementary use of CTA and MRA could reduce the discrepancy of the center coordinates from an angiography-based center. Blatt *et al.* investigated the issue of the shift of the nidus center and difference in diameter between the nidus seen on conventional stereotactic angiography and CT with intra-arterial contrast infusion in 81 AVMs (5). In 44 cases (54%), the isocenters differed by an average of 3.6 mm. Fourteen nidi were larger on CT (average, 2.6 mm), and 30 were smaller on CT (average, 4.0 mm). The authors concluded that those discrepancies could be attributed to error in the angiographic nidus determination, with factors including overlapping vessels, bony structures, fine filamentous arterioles, and an irregular shape. The distortion of DSA could be a possible source of error as well (15–17). Factors that influence the distortions are the curvature of the I/I screen ("pin-cushion distortion"), the earth's magnetic field ("S distortion"), and other external or internal magnetic fields. Pincushion distortion can be mathematically reduced, but S distortion cannot be eliminated (15). The distortion can be up to 4 mm at the edge of the image without distortion correction, although it is usually 1 mm or less for the diameter of 16–23 cm from the center of image; therefore, the contribution of the distortion correction could be minimal (16, 17).

We agree that biplanar stereotactic angiography has some limitations in the depiction of nidus, as Blatt *et al.* (5) and other authors have pointed out (1, 3, 4). However, we should be aware of the limitations of MRA and CTA, as well. One of the major drawbacks of these modalities is the limited ability of temporal resolution (18, 19). Distortion of images and some other artifacts inherent to MRA could be the result of other possible sources of error, as well (3–5, 14, 20). The distortion of MRI happens by system-related and

Table 1. Characteristics of the material and the results regarding depiction, displacement of center, coverage of angiography-based AVM by MRA-based AVM, and the ellipsoidal volume

	Images used	Location of AVM	Maximum diameter on angiography (mm)	Depiction of AVM		Displacement of centers of two modalities (mm)				Coverage of angiography-based AVM by MRA-based AVM (%)			Ellipsoidal volume (cc)	
				MRA	CTA	Left-right	Anterior-posterior	Cranio-caudal	Three-dimensional	Left-right	Anterior-posterior	Cranio-caudal	MRA	Angiography
AVM-1	MRA only	Basal ganglia	48.6	Clear	NA	1.1	−0.8	0.8	1.5	100	100	97	49.4	37.8
AVM-2	MRA only	Temporal lobe	33.8	Clear	NA	−0.7	0.2	−0.7	1.0	100	100	92	8.7	5.3
AVM-3	MRA only	Temporal lobe	26.8	Clear	NA	−4.0	2.8	1.9	5.2	80	100	100	6.4	3.2
AVM-4	MRA only	Nons	36.4	Clear	NA	−5.7	−1.4	2.3	6.3	83	96	94	15.7	14.3
AVM-5	MRA only	Thalamus	14.7	Clear	NA	−1.2	1.2	−0.1	1.7	86	92	100	1.0	0.9
AVM-6	MRA only	Temporal lobe	28.9	Clear	NA	−1.6	−1.5	3.6	4.2	100	88	92	11.4	10.6
AVM-7	MRA only	Cerebellum	20.1	Clear	NA	−1.8	−0.5	2.6	3.2	100	100	100	6.9	4.1
AVM-8	MRA only	Temporal lobe	13.8	Unclear	NA	−2.4	3.8	−0.7	4.5	69	61	94	0.6	1.0
AVM-9	MRA + CTA	Temporal lobe	38.2	Clear	Clear	−2.9	−2.0	−0.1	3.5	86	91	96	10.0	11.8
AVM-10	MRA + CTA	Frontal lobe	16.6	Clear	Clear	−1.4	−1.3	−0.4	2.0	82	97	92	1.3	1.5
AVM-11	MRA + CTA	Frontal lobe	19.1	Clear	Clear	−2.1	−5.1	−0.6	5.6	92	70	84	2.5	2.7
AVM-12	MRA + CTA	Temporal lobe	29.8	Clear	Clear	−12.4	1.6	−1.4	12.5	33	100	96	7.4	7.2
AVM-13	MRA + CTA	Eccipital lobe	10.3	Clear	Clear	−1.8	0.5	−0.1	1.9	91	91	100	0.5	0.4
AVM-14	MRA + CTA	Eccipital lobe	27.3	Clear	Clear	−0.8	5.6	2.3	6.1	100	70	90	7.5	5.7
AVM-15	MRA + CTA	Temporal lobe	27.0	Unclear	Clear	1.9	−2.4	0.1	3.1	78	100	74	3.4	4.8
AVM-16	MRA + CTA	Temporal lobe	27.0	Clear	Clear	−3.5	0.6	−1.6	3.9	85	93	90	4.6	5.3
AVM-17	MRA + CTA	Nons	9.4	Clear	Unclear	1.5	−1.0	0.6	1.9	100	83	64	0.5	0.3
AVM-18	MRA + CTA	Frontal lobe	9.4	Unclear	Clear	0.4	−0.5	1.4	1.5	100	100	83	0.4	0.3
AVM-19	MRA + CTA	Frontal lobe	10.0	Unclear	Clear	−0.2	0.0	0.0	0.2	98	99	69	0.2	0.3
AVM-20	MRA + CTA	Temporal lobe	6.6	Unclear	Clear	−1.5	−2.8	−0.1	3.2	100	62	100	0.2	0.1
AVM-21	MRA + CTA	Pons	12.1	Clear	Clear	−1.5	3.1	2.7	4.4	81	80	100	1.2	0.6
AVM-22	MRA + CTA	Eccipital lobe	35.4	Unclear	Clear	−2.0	−1.0	0.0	2.2	100	100	100	18.7	10.3
AVM-23	MRA + CTA	Parietal lobe	44.7	Clear	Unclear	0.5	7.4	8.6	11.3	88	80	76	27.6	35.7
AVM-24	MRA only	Temporal lobe	45.3	Clear	NA	−2.0	0.8	4.0	4.5	82	100	88	27.9	30.6
AVM-25	MRA only	Cerebellum	67.1	Clear	NA	0.0	3.6	−0.1	3.6	92	97	93	97.2	118.1
AVM-26	MRA only	Temporal lobe	31.8	Clear	NA	−3.7	−3.3	0.4	5.0	99	94	100	15.6	8.9
AVM-27	MRA only	Frontal lobe	30.7	Unclear	NA	−2.1	−9.0	−2.0	9.4	86	100	83	14.4	11.7
AVM-28	MRA only	Temporal lobe	10.7	Clear	NA	−1.1	−0.8	2.2	2.6	100	100	100	3.3	0.5

Abbreviations: AVM = arteriovenous malformation; MRA = magnetic resonance angiography; CTA = computed tomographic angiography; NA = not applicable.

Table 2. The impact of CTA in addition to MRA for the targeting, regarding the degree of the displacement of centers between MRA(± CTA)-based AVMs and angiography-based AVMs

		Distance of centers between angiography-based AVM and MRA(±)CT-based AVM (mm)							
The use of CTA	*n*	LR direction	*p*	AP direction	*p*	CC direction	*p*	3D	*p*
No	13	2.07	0.81	3.59	0.37	1.66	0.64	5.32	0.47
Yes	15	2.29		2.33		1.33		4.22	

Abbreviations: CTA = computed tomographic angiography; MRA = magnetic resonance angiography; AVM = arteriovenous malformation; LR = left-right; AP = anterior-posterior; CC = craniocaudal.

object-related causes, and it can be as large as 4–5 mm at the edge of the magnetic field (14, 20). System-related distortion can be reduced by the modification of k-space data; however, its contribution is small as far as brain lesions are concerned, because the distortion is usually submillimetric around the center of the magnetic field without distortion correction (14).

The results of the present study suggest that the target on MRA or CTA might have included an unnecessary area of the AVM (the feeding artery or draining vein) but missed an important portion (the nidus), probably because of the poor temporal resolution of MRA.

Therefore, our supposition is that DSA still remains the basic source for 3D information to delineate the nidus and to discriminate the feeding arteries and draining veins from the nidus. Two groups have recently reported the advanced use of DSA for targeting purposes. Colombo *et al.* developed a novel system of integrating nonstereotactic 3D rotational angiography with stereotactic CT scanning (18). They used their system in 20 patients, and the result was compared with that obtained by conventional biplanar stereotactic angiography. For each patient, the number of isocenters and the dimension of the selected collimators were the same, based on the information supplied by both methods. Target coordinates were modified in 5 cases by a very limited amount (mean, 0.7 mm; range, 0.3–1.0 mm). Zhang *et al.* reconstructed a biplanar stereotactic DSA to a three-dimensional fashion (segmented DSA), and then complementarily used 3D information in the targeting

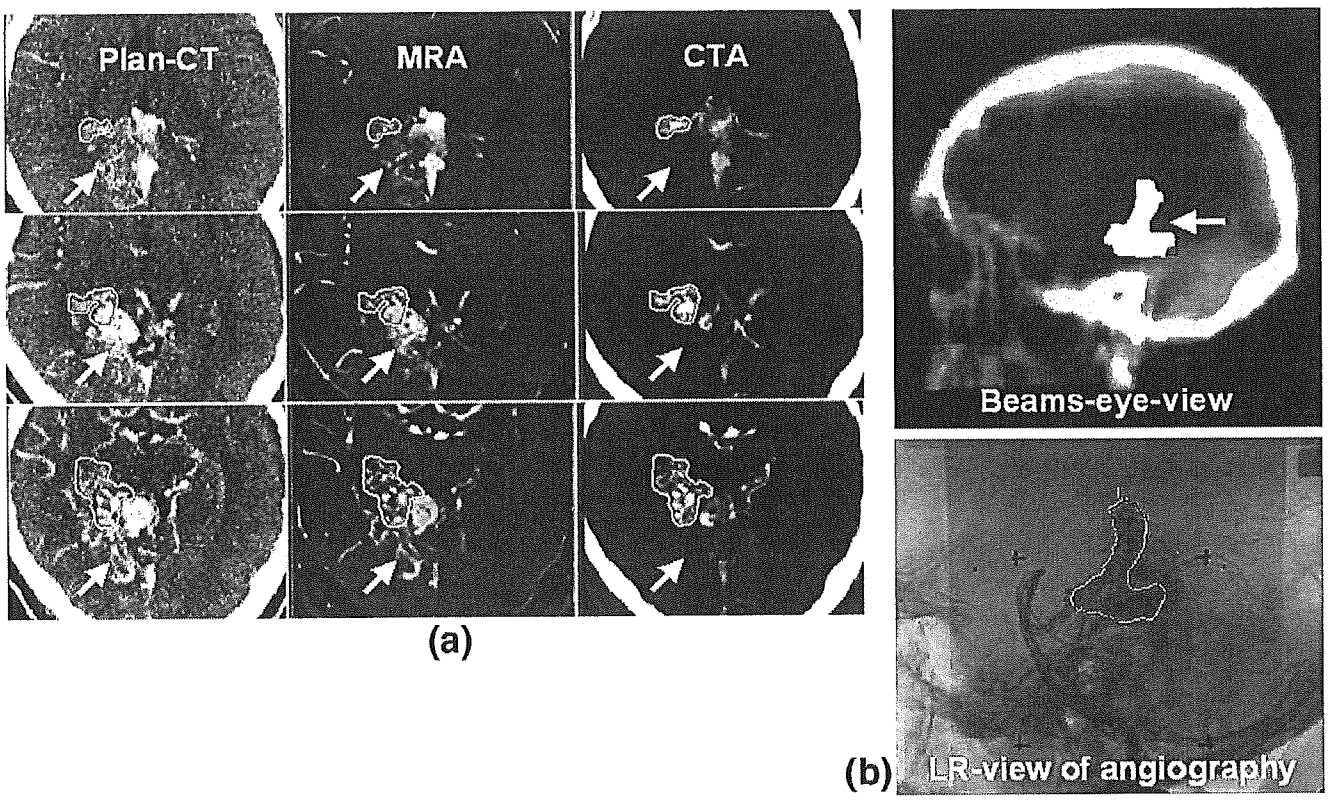

Fig. 4. An example of the improvement of the target shape with the information obtained by computed tomographic angiography (CTA): (a) The posterior part of the arteriovenous malformation (AVM) (arrow) was omitted from the target after the integration of the CTA information. (b) The resultant beam's-eye–view showed good correlation with the left-right (LR) view of stereotactic angiography.

process (19). The shift of center between the targets determined on the segmented DSA plus the enhanced CT and classic stereotactic DSA was 0.1–0.2 mm in any direction. Because the shift of centers when the MRA or CTA was used was 2–4 mm in our series and in the series by Blatt *et al.* (5), using advanced 3D angiography as shown by Colombo *et al.* (18) and Zhang *et al.* (19) is recommended to improve the accuracy of target delineation.

In conclusion, the use of MRA or CTA provided important 3D information for target determination, but the shift of center between MRA and stereotactic DSA and inadequate coverage of angiography-based target by MRA-based target were not negligible. Therefore, DSA should be the basic source for 3D information to delineate the nidus. If the target is delineated using an MRA, it is important to understand the limitations of the MRA, to ensure delineation of the nidus and to exclude unnecessary structures in the target volume.

REFERENCES

1. Spiegelmann R, Friedman WA, Bova FJ. Limitations of angiographic target localization in planning radiosurgical treatment. *Neurosurgery* 1992;30:619–623.
2. Aoyama H, Shirato H, Nishioka T, *et al.* Treatment outcome of single or hypofractionated single-isocentric stereotactic irradiation (STI) using a linear accelerator for intracranial arteriovenous malformation. *Radiother Oncol* 2001;59:323–328.
3. Bednarz G, Downes B, Werner-Wasik W, *et al.* Combining stereotactic angiography and 3D time-of-flight magnetic resonance angiography in treatment planning for arteriovenous malformation radiosurgery. *Int J Radiat Oncol Biol Phys* 2000;46:1149–1154.
4. Kondziolka D, Lunsford LD, Kanal E, *et al.* Stereotactic magnetic resonance angiography for targeting in arteriovenous malformation radiosurgery. *Neurosurgery* 1994;35:585–591.
5. Blatt DR, Friedman WA, Bova FJ. Modifications based on computed tomographic imaging in planning the radiosurgical treatment of arteriovenous malformation. *Neurosurgery* 1993; 33:588–596.
6. Schad LR. Improving target volume characterization in stereotactic treatment planning of brain lesions by using high-resolution BOLD MR-venography. *NMR Biomed* 2001;41: 478–483.
7. Farb RI, McGregor C, Kim JK, *et al.* Intracranial arteriovenous malformations: Real-time auto-triggered elliptic centric-ordered 3D gadolinium-enhanced MR angiography—initial assessment. *Radiology* 2001;220:244–251.
8. Essig M, Engenhart R, Knopp MV, *et al.* Cerebral arteriovenous malformations: Improved nidus demarcation by means of dynamic tagging MR-angiography. *Magn Reson Imaging* 1996;14:227–233.
9. Morikawa M, Numaguchi Y, Rigamonti D, *et al.* Radiosurgery for cerebral arteriovenous malformations: Assessment of early phase magnetic resonance imaging and significance of gadolinium-DTPA enhancement. *Int J Radiat Oncol Biol Phys* 1996;34:663–675.
10. Guo WY, Nordell B, Karlsson B, *et al.* Target delineation in radiosurgery for cerebral arteriovenous malformations. Assessment of the value of stereotaxic MR imaging and MR angiography. *Acta Radiol* 1993;34:457–463.
11. George EJS, Butler P, Plowman PN. Can magnetic resonance imaging alone accurately define the arteriovenous nidus for gamma knife radiosurgery? *J Neurosurg* 2002;97:464–470.
12. Tanaka H, Numaguchi Y, Konno S, *et al.* Initial experience with helical CT and 3D reconstruction in therapeutic planning of cerebral AVMs: Comparison with 3D time-of-flight MRA and digital subtraction angiography. *J Comput Assist Tomogr* 1997;21:811–817.
13. Shidon RL, Barth NH. Stereotactic localization of intracranial targets. *Int J Radiat Oncol Biol Phys* 1987;13:1241–1246.
14. Aoyama H, Shirato H, Nishioka T, *et al.* Magnetic resonance imaging system for three-dimensional conformal radiotherapy and its impact on gross tumor volume delineation of central nervous system tumors. *Int J Radiat Oncol Biol Phys* 2001; 50:821–827.
15. Soderman M, Picard C, Ericson K. An algorithm for correction of distortion in stereotaxic digital subtraction angiography. *Neuroradiology* 1998;40:277–282.
16. Wu TH, Lee JS, Wu HM, *et al.* Evaluating geometric accuracy of multi-platform stereotactic neuroimaging in radiosurgery. *Stereotact Funct Neurosurg* 2002;78:39–48.
17. Perks J, St George EJ, Doughty D, *et al.* Is distortion correction necessary for digital subtraction angiography in the gamma knife treatment of intra-cranial arteriovenous malformation? *Stereotact Funct Neurosurg* 2001;76:94–105.
18. Colombo F, Cavedon C, Francescon P, *et al.* Three-dimensional angiography for radiosurgical treatment planning for arteriovenous malformations. *J Neurosurg* 2003;98:536–543.
19. Zhang XQ, Shirato H, Aoyama H, *et al.* Clinical significance of 3D reconstruction of arteriovenous malformation using digital subtraction angiography and its modification with CT information in stereotactic radiosurgery. *Int J Radiat Oncol Biol Phys* 2003;57:1392–1399.
20. Khoo VS, Dearnaley DP, Finnigan DJ, *et al.* Magnetic resonance image (MRI): Considerations and applications in radiotherapy treatment planning. *Radiother Oncol* 1997;42:1–5.

INSTITUTE OF PHYSICS PUBLISHING PHYSICS IN MEDICINE AND BIOLOGY

Phys. Med. Biol. **50** (2005) 3655–3667 doi:10.1088/0031-9155/50/16/001

Residual motion of lung tumours in gated radiotherapy with external respiratory surrogates

Ross I Berbeco[1], Seiko Nishioka[2], Hiroki Shirato[3], George T Y Chen[1] and Steve B Jiang[1]

[1] Department of Radiation Oncology, Massachusetts General Hospital and Harvard Medical School, Boston, MA, USA
[2] Department of Radiology, NTT Hospital, Sapporo, Japan
[3] Department of Radiation Medicine, Hokkaido University School of Medicine, Sapporo, Japan

E-mail: rberbeco@partners.org

Received 15 March 2005, in final form 24 May 2005
Published 28 July 2005
Online at stacks.iop.org/PMB/50/3655

Abstract

Due to respiration, many tumours in the thorax and abdomen may move as much as 3 cm peak-to-peak during radiation treatment. To mitigate motion-induced irradiation of normal lung tissue, clinics have employed external markers to gate the treatment beam. This technique assumes that the correlation between the external surface and the internal tumour position remains constant inter-fractionally and intra-fractionally. In this work, a study has been performed to assess the validity of this correlation assumption for external surface based gated radiotherapy, by measuring the residual tumour motion within a gating window. Eight lung patients with implanted fiducial markers were studied at the NTT Hospital in Sapporo, Japan. Synchronized internal marker positions and external abdominal surface positions were measured during the entire course of treatment. Stereoscopic imaging was used to find the internal markers in four dimensions. The data were used retrospectively to assess conventional external surrogate respiratory-gated treatment. Both amplitude- and phase-based gating methods were investigated. For each method, three gating windows were investigated, each giving 40%, 30% and 20% duty cycle, respectively. The residual motion of the internal marker within these six gating windows was calculated. The beam-to-beam variation and day-to-day variation in the residual motion were calculated for both gating modalities. We found that the residual motion (95th percentile) was between 0.7 and 5.8 mm, 0.8 and 6.0 mm, and 0.9 and 6.2 mm for 20%, 30% and 40% duty cycle windows, respectively. Five of the eight patients showed less residual motion with amplitude-based gating than with phase-based gating. Large fluctuations (>300%) were seen in the residual motion between some beams. Overall, the mean beam-to-beam variation was 37% and 42% from the previous treatment beam for amplitude- and phase-based gating, respectively. The day-to-day variation was 29% and 34% from the previous day for amplitude- and phase-based gating, respectively.

0031-9155/05/163655+13$30.00

Although gating reduced the total tumour motion, the residual motion behaved unpredictably. Residual motion during treatment could exceed that which might have been considered in the treatment plan. Treatment margins that account for motion should be individualized and daily imaging should be performed to ensure that the residual motion is not exceeding the planned motion on a given day.

(Some figures in this article are in colour only in the electronic version)

1. Introduction

Many tumours in the abdomen and thorax have been observed to move during respiration (Weiss *et al* 1972, Bryan *et al* 1984, Suramo *et al* 1984, Ross *et al* 1990, Davies *et al* 1994, Balter *et al* 1996, Ekberg *et al* 1998, Shimizu *et al* 1999, Langen and Jones 2001). Several respiratory motion compensation strategies have been proposed to minimize harmful effects (Ohara *et al* 1989, Maruhashi *et al* 1992, Kubo and Hill 1996, Wong *et al* 1999, Minohara *et al* 2000, Schweikard *et al* 2000, Shirato *et al* 2000a, Barnes *et al* 2001, Keall *et al* 2001, Harada *et al* 2002, Kubo and Wang 2002, Zhang *et al* 2003, Berbeco *et al* 2004, Mageras and Yorke 2004). In approaches that gate the beam with no interruption of patient breathing, physiologically based surrogates of tumour location are used to trigger the therapeutic beam. Shirato *et al* (2000a) have reported a method for gating based on the three-dimensional location of a fiducial implanted near the tumour. Berbeco *et al* (2004) have suggested the use of fluoroscopic images for gating based exclusively on motion-enhanced tumour images, without implanted surrogates. Although these methods explicitly ensure that the location of the tumour is within the gating window, concerns of imaging dose, complexity or expense may discourage users. Several institutions and companies have developed techniques for respiratory gating based on the position of an external surrogate (or a collection of surrogates) placed on the thorax and/or abdomen. These systems do not require fluoroscopy during treatment. However, there is some uncertainty as to how well monitoring an external surface can predict internal tumour location as a function of time. Schweikard *et al* (2000) used infrared external markers and implanted radiopaque markers to periodically re-establish the internal/external correlation throughout a lengthy Cyberknife system (Accuray, Inc., Sunnyvale, CA) irradiation session. This may also suffer the same concerns, depending on the imaging frequency and total length of the treatment.

The question is: for regular linac based treatments, is an external surrogate alone sufficient for precise gated lung treatment? We use the measured patient data to examine this question. The residual tumour motion is calculated for several external gating duty cycles for the whole treatment. Beam-to-beam and day-to-day variations in the residual motion are also calculated. We comment on the reliability of external surrogate-based respiratory gating on these time scales.

2. Methods and materials

2.1. The patients

A total of eight lung patients were studied. The details of each patient are given in table 1. Patients 1–3 were brought to the NTT Hospital for the specific purpose of acquiring data for this study. Data were taken for only a single day for these patients. Patients 4–8 were treated

Table 1. Information about the patients studied. Patient 5 was treated twice, at the same site, with 2 months between treatments. The tumour site is indicated using the common anatomical notation for lung segmentation: S1–3 is upper lobe, S4–5 is middle lobe and S6–10 is lower lobe.

Patient	Gender	Age	Tumour pathology	Number of bb's	Tumour site	Prescribed dose (Gy)	Fractions
1	F	47	Adenocarcinoma	4	Rt. S7	N/A	1
2	F	70	Adenocarcinoma	3	Lt. S6	N/A	1
3	F	71	Adenocarcinoma	2	Rt. S5	N/A	1
4	F	47	Adenocarcinoma	3	Rt. S4	48	8
5	M	81	Squamous cell carcinoma	3	Rt. S2b	48	4
5						40	8
6	M	61	Small cell lung cancer	3	Rt. S10	40	8
7	M	68	Squamous cell carcinoma	3	Rt. S6	48	4
8	M	85	Adenocarcinoma	3	St. S8	48	4

with 40–48 Gy in four to eight fractions. This analysis only includes patients with marker motion greater than 1 cm peak-to-peak. Patient 5 was treated twice, 2 months apart. Since the same site was treated and no isocentre shift was made, we used both sets of data in the evaluation, under the same patient name. Some beams/day were excluded because the patient shifted during treatment.

2.2. *External and internal gating systems*

The Radiation Oncology Clinic at the Nippon Telegraph and Telephone Corporation (NTT) Hospital in Sapporo, Japan, is equipped with a Mitsubishi real-time radiation therapy (RTRT) system (Shirato *et al* 2000a). Patients with abdominal and thoracic tumours, treated with this system, typically have two to four 1.5 mm diameter gold ball bearings (bb's) implanted in or near the tumour (Shirato *et al* 2003). These markers are tracked in real time with diagnostic x-ray fluoroscopy, and the treatment beam turned on when a marker is within a predetermined 3D window (Shirato *et al* 2000a). The routine practice is to use a 3D window that is ± 2.5 mm from the planned position in each direction (LR, SI and AP). The system at the NTT Hospital differs from the usual RTRT system in that there are only two pairs of x-ray tubes and imagers rather than four. Therefore, at some gantry angles, one of the x-ray views may be blocked. To facilitate gating at these angles, an external surrogate gating system was installed and integrated with the RTRT system by Mitsubishi. The AZ-733V external respiratory gating system (Anzai Medical, Tokyo, Japan) uses a laser to monitor the movement of the patient's abdominal surface. The housing, which contains both the source and the detector, is attached to the treatment couch by an extendable arm and the beam is placed orthogonal to the patient's skin surface. The device calculates the change in the surface amplitude by measuring the relative position of the reflected light. The result is a 1D relative measurement of the abdominal surface. For the purposes of this study, the external surface was monitored when neither of the x-ray views was obscured. The signal from the surface monitor is synchronized with the signal from the fluoroscopic unit so that the log files contain the three-dimensional marker position and the external surface position at every time point. The rate of data acquisition for this entire system is 30 frames s^{-1}. Note that the fluoroscopic and laser measurements are taken even when the treatment beam is gated off. Data are acquired throughout each treatment, so we were able to obtain large amounts of internal/external correlated data.

2.3. Patient setup

In the CT simulation session, a scan is taken with the patient's breath held at the end of exhale. At each treatment session, patients are initially set up to skin marks using in-room lasers. Short fluoroscopic imaging sessions are performed to determine the position of the markers at the end of exhale phase. The 3D marker position is compared to the planned position. The RTRT system then calculates the appropriate couch shift (performed by the therapist) to bring the target to isocentre. The physician monitors the fluoroscopy to verify that the markers are properly tracked and are within the internal gating window at the end of exhale. A complete description of the treatment procedure has been written by Shirato *et al* (2000).

The accuracy of externally gated treatment can be broken up into two factors: (1) daily variation of tumour home position (e.g. end-of-exhale tumour position) and (2) residual motion of the tumour within the external gating window. In a gated treatment procedure, the patient is set up such that, at the end of exhale, the tumour is at the reference home position. Therefore, the setup is not only *patient* positioning but also *tumour* positioning. If the patient is accurately positioned, based on the end-of-exhale tumour location before each fraction of treatment, then day-to-day error is minimized. During data taking for this study, fluoroscopy was taken prior to each treatment to ensure that the implanted markers were at the planned positions at the end of exhale. This method allows us to set aside the errors associated with patient setup and inter-fractional tumour motion and focus on those uncertainties arising from internal residual tumour motion within the external gating window throughout the treatment.

2.4. Data analysis

The data acquired by both the internal and external monitoring systems indicate a 'position' at each time step. For the external monitoring system, the position is the distance from the abdominal surface to the laser housing. In the internal monitoring system, the position of the tracked marker is calculated in isocentre coordinates. To calculate the phase of the external signal for each time point, a retrospective algorithm is employed (Neicu *et al* 2003). The end of inhale is assigned phase angle $0/2\pi$ degrees and the phase angle of exhale is generally around π, depending on the shape of the breathing waveform.

Residual tumour motion is assessed for two gating strategies: amplitude-based gating and phase-based gating. It has been noted in the literature that there are potential problems with each of these methodologies, which may be tied to issues of correlation. Each method can be problematic if a patient's depth of breathing is inconsistent. A patient's breathing waveform may experience a baseline drift, potentially causing the beam to turn on during an unintended interval (Mageras and Yorke 2004). In phase-based gating, shallow exhales will trigger a beam at different amplitudes than deeper exhales (see figure 1).

2.4.1. Amplitude-based gating. In this study, we have chosen the gating amplitude window to encompass patient's end of exhalation. The gate is open when the external amplitude falls below a predefined level. Gating windows were chosen for each beam such that the duty cycle was 20%, 30% or 40%, respectively. The gating windows were chosen such that the lower part of the gate was always less than the minimum of the amplitude. The residual motion is defined to be the motion of internal markers during the open external gating window. For each beam, there will be a 3D collection of data points representing the positions of the internal marker when the external amplitude was within the gating window. The median of these points (the median gated position) is the reference point from which r_{internal} is calculated. r_{internal} is the magnitude of the 3D distance between each gated data point and the median gated position. A representative plot of r_{internal} for amplitude-based gating is shown in figure 2(a).

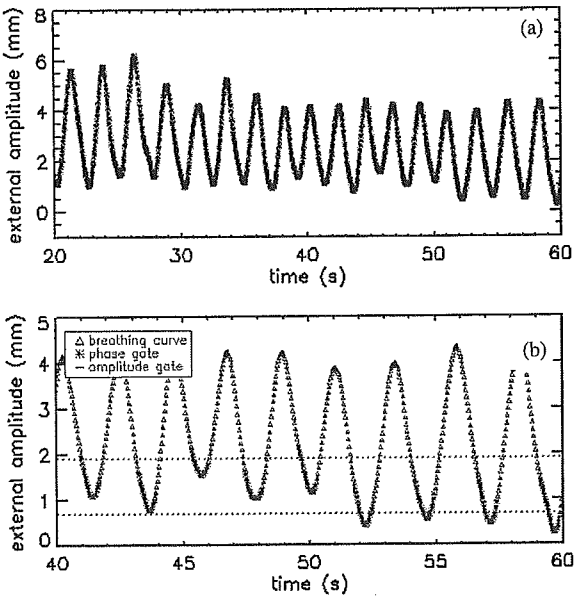

Figure 1. (a) The amplitude of the external surface of a patient is shown as a function of time. The amplitude of exhale (minima) can change through the course of even a relatively short session like this one. (b) To show how the changing amplitude of the minima can affect gating, 20 s of the breathing curve is shown with the phase-gated points represented by blue asterisks and the amplitude-gating window by the red dotted lines (both for 30% duty cycle).

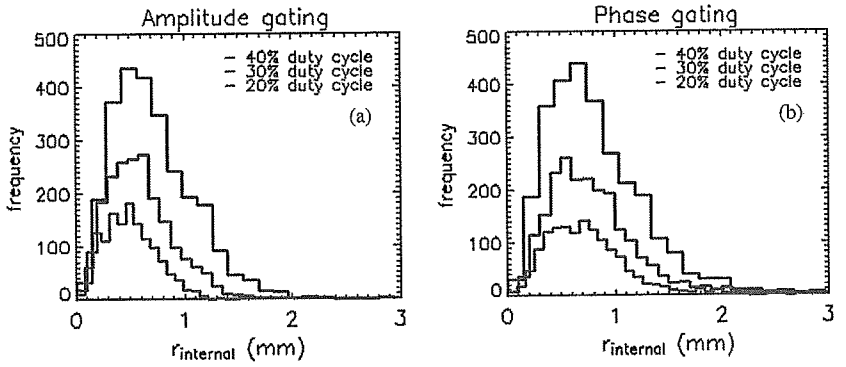

Figure 2. Representative histograms of the residual motion for 40% (black), 30% (blue) and 20% (red) duty cycle for (a) amplitude-based gating and (b) phase-based gating for patient 5.

2.4.2. Phase-based gating. A similar analysis is performed for phase-based gating. The phase for the gating window is found by an exhaustive search of all phase angle windows in 0.1 radian increments. The gates are selected which result in the lowest residual motion for 20%, 30% and 40% duty cycle. This represents the best possible phase gating region for each duty cycle. These gating regions tended to be near the end of exhale. The residual motion is defined to be the collection of internal data points corresponding to the external gating window. The median of these points (the median gated position) is the reference point from which $r_{internal}$ is calculated. A representative plot of $r_{internal}$ for phase-based gating is shown in figure 2(b).

Table 2. The mean and 95th percentile residual motion at 20%, 30% and 40% for amplitude- and phase-based gating (d.c. = duty cycle, A = amplitude-based gating, P = phase-based gating and n = negligible motion).

		Mean residual motion (mm)						95th percentile residual motion (mm)					
	Total internal motion (mm)	20% d.c.		30% d.c.		40% d.c.		20% d.c.		30% d.c.		40% d.c.	
Patient	LR/SI/AP	A	P	A	P	A	P	A	P	A	P	A	P
1	n/19/6	0.8	1.3	0.9	1.4	1.2	1.7	1.6	2.9	2.0	3.2	2.3	3.6
2	n/13/n	0.9	0.9	1.1	0.9	1.2	1.1	2.1	2.1	2.6	2.2	3.0	2.6
3	5/5/9	1.2	0.8	1.2	0.9	1.5	1.1	3.5	1.4	4.1	1.6	4.4	1.9
4	n/10/6	0.7	0.5	0.7	0.7	0.8	0.8	2.0	1.1	1.8	1.4	1.6	1.7
5	n/10/5	0.5	0.8	0.6	0.8	0.7	0.8	0.9	1.4	1.1	1.5	1.3	1.6
6	n/12/n	1.1	1.6	1.2	1.7	1.4	1.8	2.7	4.7	3.1	4.8	3.6	5.1
7	n/10/n	0.4	0.4	0.4	0.4	0.5	0.5	0.7	0.7	0.9	0.8	1.0	0.9
8	n/15/6	1.6	2.7	1.9	2.8	2.1	3.0	3.0	5.8	3.7	6.0	4.2	6.2

3. Results and discussion

3.1. Range of residual motion

The 95th percentile of residual motion in a 40% duty cycle window is chosen as the metric by which we judge the efficacy of gating. This makes our discussion of the results easier to present. Inspecting table 2, five of the patients (1, 4, 5, 6 and 8) show reduced residual motion with amplitude gating versus phase-based gating. The other patients show the contrary, although each to varying degrees. Overall, in this group of patients, neither amplitude-based gating nor phase-based gating is definitively better than the other. Three patients (4, 5 and 7) have small residual motion (<2.5 mm) for both gating modalities, even at 40% duty cycle. Patient 2 also shows similar results for both modalities but with slightly more motion. Patient 3 has significantly less residual motion with phase-based gating (<2 mm). The residual motion for each patient does not appear to be well correlated with the size of the total motion (un-gated). Although patient 1 has the largest un-gated motion, patients 6 and 8 have more residual motion for both modalities and patients 2 and 3 have more for amplitude-based gating. Total motion does not appear to be a good predictor of the size of the residual motion.

Only patient 3 exhibits significant motion in all three directions. The 95th percentile residual motion histograms for the LR, SI and AP directions are shown in figure 3. The tail in the posterior direction in the amplitude gating, for patient 3, gives rise to the larger residual motion for this modality. The external amplitude as a function of the internal motion in the AP direction is shown in figure 4(a). Amplitude gating accepts a wider range of data in the AP direction than phase-based gating. External amplitude versus external phase is shown in figure 4(b). The phase-based gating prefers points on the exhalation side of the minimum (i.e. left of the minimum). Given that the phase-based gating leads to less residual motion for this patient, figure 4(b) implies that external phase correlates better with internal motion than external amplitude. This does not appear to be true for all of the other patients.

Patients 1, 6 and 8 have significantly less residual motion with amplitude-based gating compared to phase-based gating (38%, 29% and 32% less, respectively). Plots of the external amplitude as a function of the internal motion in the SI direction for patient 6 are shown in figure 5. To better see in which phase direction the gated phase points are, external amplitude

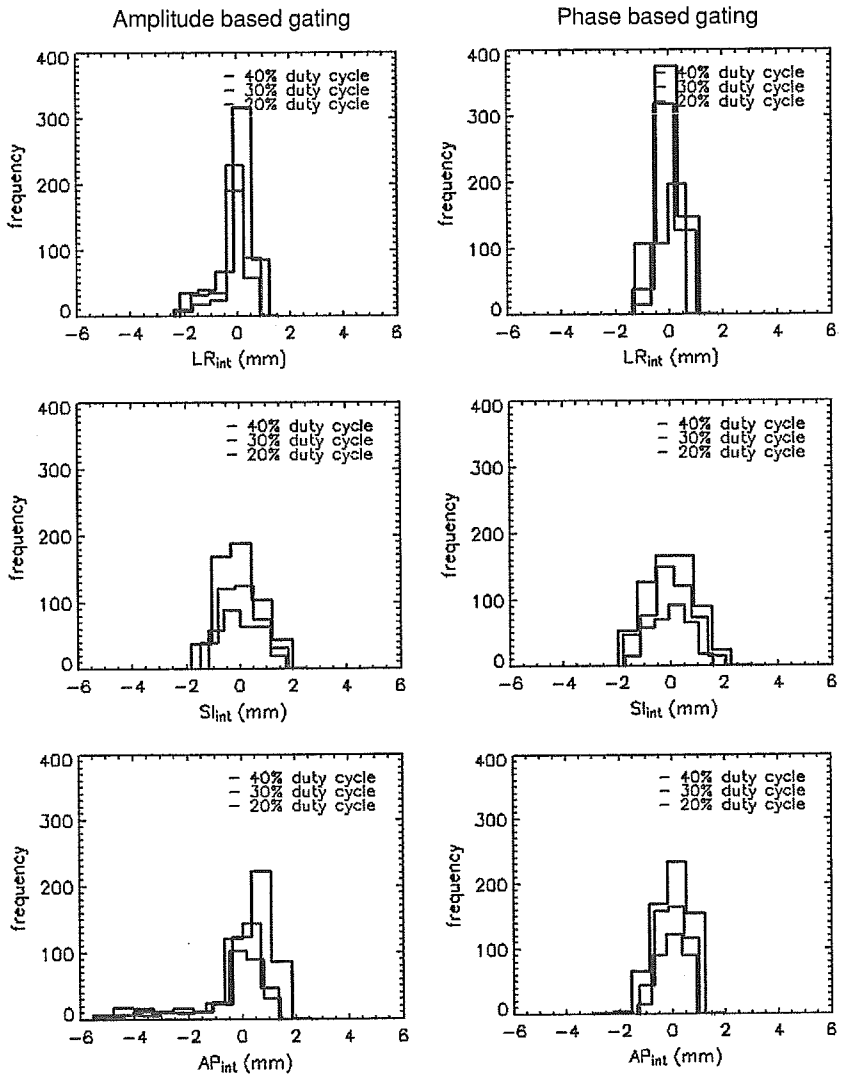

Figure 3. Histograms of the internal residual motion in the LR, SI and AP coordinates for amplitude- and phase-based gating for patient 3. Note the longer tail in the posterior direction for amplitude-based gating.

is plotted as a function of external phase for all three patients (1, 6 and 8) in figures 6(a)–(c). The phase-gated points extend beyond the amplitude-gated points in both inhale and exhale directions. The large width of the collection of data points near the minimum leads to phase-based gated points beyond the amplitude gate. The width is a measure of the reproducibility of the phase/amplitude relationship. This relationship can be made more reproducible through breath coaching (Mageras *et al* 2001, Kini *et al* 2003, Neicu *et al* 2004). However, there is no evidence, yet, that breath coaching has a significant effect on the reproducibility of the tumour motion itself. Patients with seriously compromised pulmonary function can have inconsistent breathing. We have noticed that these patients are the most difficult to coach. It is a catch-22: the very patients for whom breath coaching may have the most benefit are those who cannot be

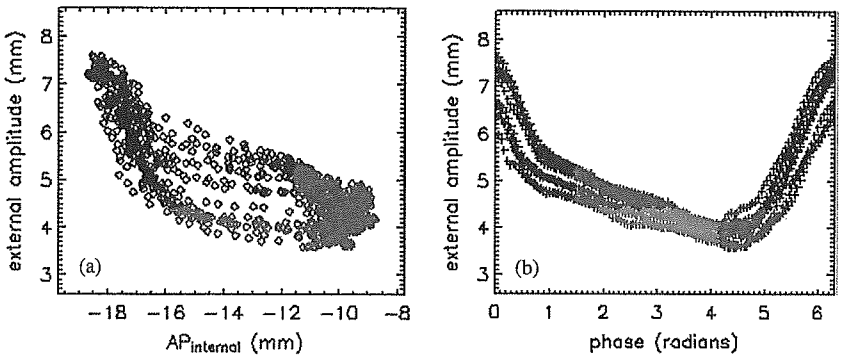

Figure 4. (a) The external amplitude as a function of internal motion in the AP direction for patient 3. The amplitude-gated points (red) are plotted over the phase-gated points (blue). (b) The external amplitude as a function of the external phase for patient 3. The phase-gated points are blue, the amplitude-gated points are red and points representing the union of the two are green. A 40% duty cycle is used for both of these plots for both phase and amplitude gating.

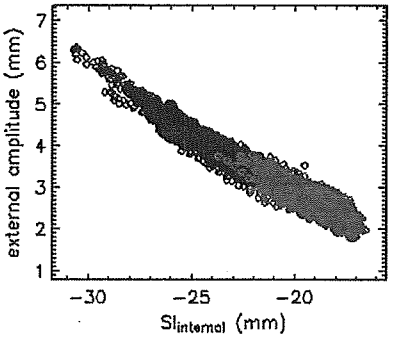

Figure 5. The external amplitude as a function of internal motion in the SI direction in shown for patient 6, day 1, beam 4. The amplitude-gated points (red) are plotted over the phase-gated points (blue). A duty cycle of 40% was used for both phase and amplitude gating.

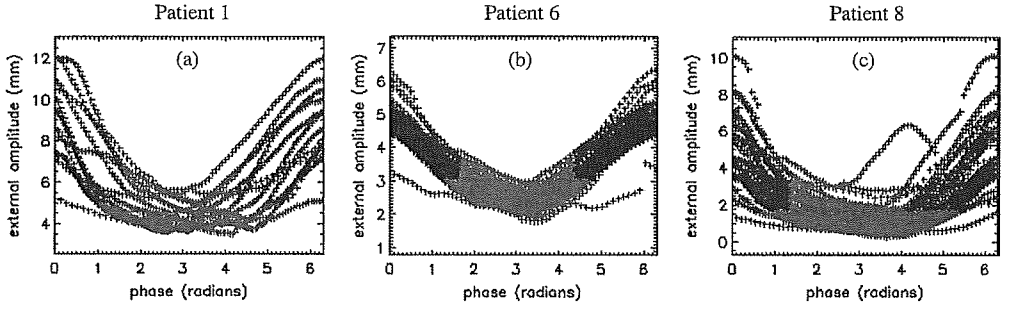

Figure 6. (a–c) The external amplitude is plotted as a function of the external phase for patients 1, 6 and 8, respectively. The amplitude-gated points (red) are plotted over the phase-gated points (blue). A duty cycle of 40% is used for all of these plots.

coached. In the absence of breath coaching, amplitude-based gating is best for the inconsistent breathers (patients 1, 6 and 8) in our group. Even so, the residual motion for these patients is still among the highest.

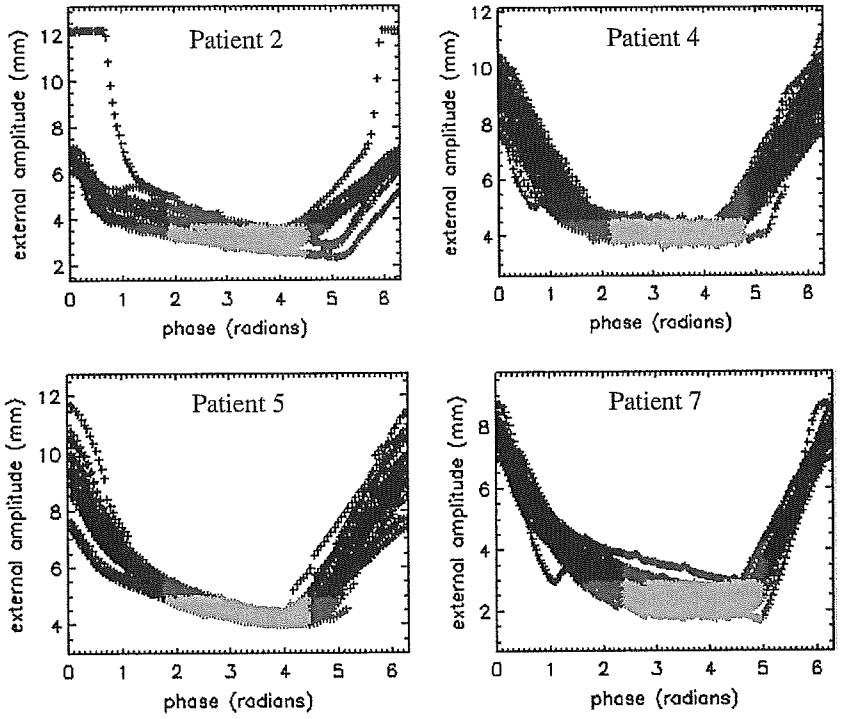

Figure 7. The external amplitude is plotted as a function of the external phase for patients 2, 4, 5 and 7. The phase-gated points are blue, the amplitude-gated points are red and points representing the union of the two are green. A duty cycle of 40% was used for all of these plots.

Patients 2, 4, 5 and 7 show the least difference in residual motion between amplitude- and phase-based gating. Patients 2 and 7 have 13% and 11% less motion, respectively, with phase-based gating versus amplitude-based gating. Patients 4 and 5 have 6% and 18% less residual motion, respectively, with amplitude-based gating versus phase-based gating. Plots of the external amplitude as a function of external phase are shown in figures 7(a)–(d). Note that even though the resulting residual motions are similar, there are still portions of the gated points that are different. Patients 2 and 5 show a preference for phases on the exhale side of the minimum, like patient 3. However, the preference is not pronounced enough to give the same residual motion effect. Patients 4 and 7 show the opposite preference. No definitive phase/amplitude relationship can be deduced from these contradictory results. The correlation between internal motion and external phase and external amplitude varies across the population of patients studied. There is no clear universal preference for one gating modality over the other.

3.2. Variation in residual motion

We studied the variability of the residual motion, beam-to-beam and day-to-day, throughout the course of treatment. For this part of the study, the first three patients were not analysed. The residual motion as a function of beam and as a function of day for each patient is shown in figures 8 and 9 for amplitude- and phase-based gating, respectively. Large changes in the residual motion are possible from beam to beam. Day 3 for patient 6 goes from beam 10 to beam 14. When amplitude gating, there is an increase of 327% between beams 10 and 11 and then a gradual decrease through the rest of that day's beams. We found that, among all

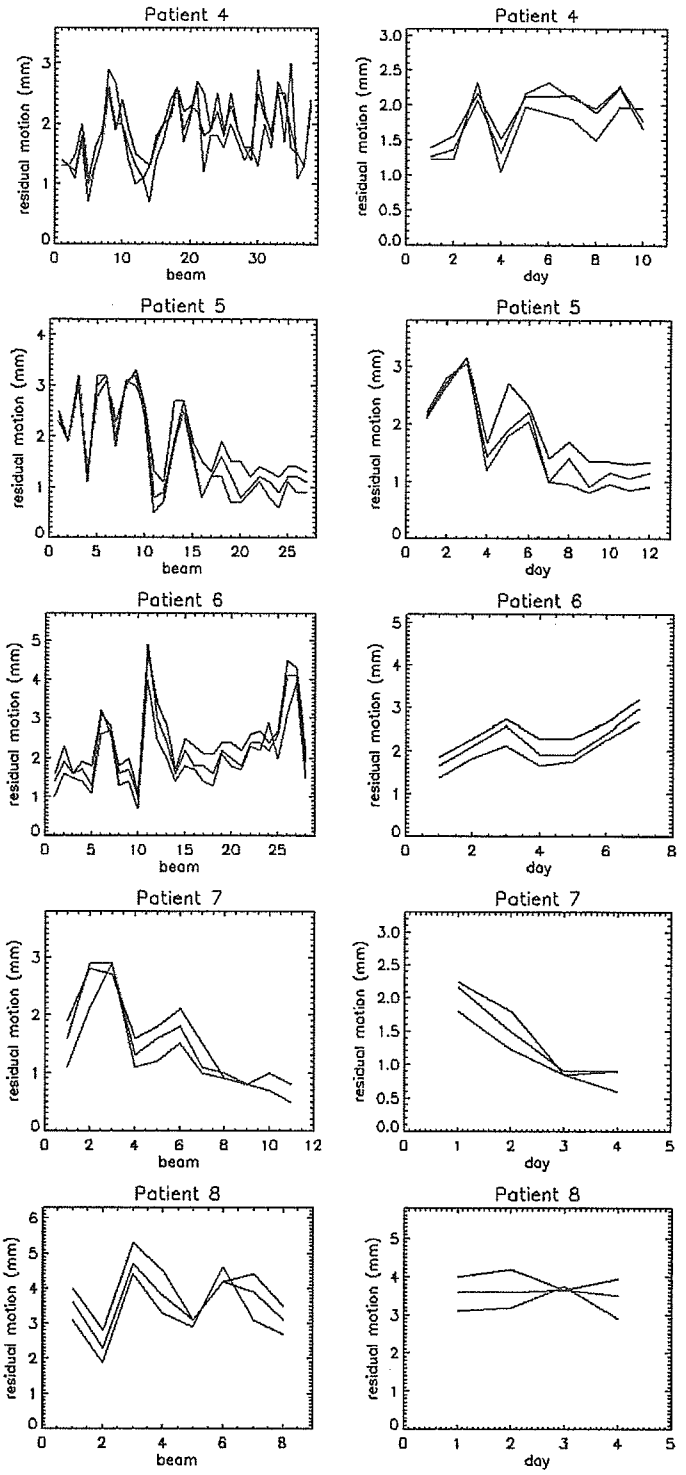

Figure 8. The 95th percentile residual motion is plotted as a function of beam, in the left column, and day, in the right column, for amplitude-based gating. The results for the 40% (black), 30% (blue) and 20% (red) duty cycles are shown.

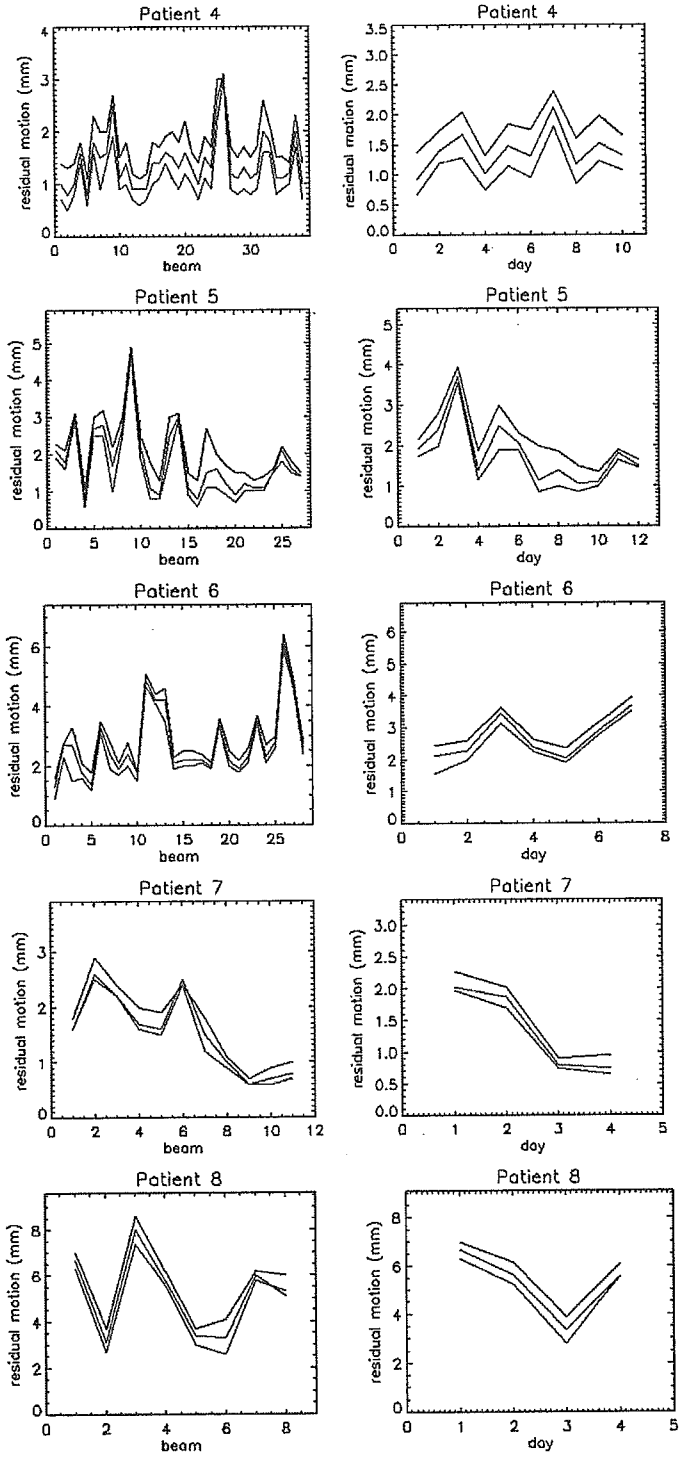

Figure 9. The 95th percentile residual motion is plotted as a function of beam, in the left column, and day, in the right column, for phase-based gating. The results for the 40% (black), 30% (blue) and 20% (red) duty cycles are shown.

the patients, the mean change from beam to beam was 37% for amplitude gating and 42% for phase-based gating. In general, each patient showed similar beam-to-beam changes for both gating modalities.

The residual motion was averaged over each day to study the daily change. The average daily residual motion change from the previous day was 25%, 30%, 17%, 48% and 9% for amplitude-based gating and 31%, 35%, 26%, 48% and 43% for patients 4–8, respectively. The average over all of the patients is 29% and 34% for amplitude- and phase-based gating, respectively. Patient 6 shows a general trend towards increasing residual motion as the treatment progresses for both gating modalities. Patients 5 and 7 show a decrease in residual motion through the course of treatment. The rest of the patients do not appear to have a noticeable trend in either direction for both gating modalities. It is unclear what factors could lead to a systematic change in the residual motion over several days.

The large fluctuations in residual motion that occur intra-fractionally and inter-fractionally are cause for concern. If one were to use an external gating system without any daily imaging, there would be no way to detect change in the residual tumour motion. Even at the same external duty cycle, the tumour may exhibit more or less motion on a given day. Treatment margins deduced from a simulation session before the course of treatment is begun may not be appropriate for each fraction. The use of inappropriate margins could lead to under-dosing of the target and/or over-dosing of the normal tissue. The dosimetric effect of the changing residual motion has not yet been studied. We highly recommend daily imaging of the patient to ensure that the tumour is moving as expected during treatment.

4. Conclusion

Residual tumour motion during external surrogate respiratory gating for both amplitude- and phase-based gating has been studied in eight patients. The data were taken over the complete course of treatment for five lung cancer patients and on a single day for three lung cancer patients. Neither gating modality proved to be definitively superior from a residual motion perspective. The significant reduction in residual motion for three of the patients using amplitude-based gating appears to be due to the irreproducibility of the breathing waveform. This will be the basis of future studies.

Overall, every patient exhibited significant reduction of the tumour motion for external gating. The variation in residual motion from patient to patient indicates that margins associated with residual tumour motion should be prescribed on a case-by-case basis. A single margin will not be appropriate for all gating patients. The tumour motion should be observed in a simulation session and an appropriate, individualized, gating window assigned before the beginning of treatment. However, our results show that the gating window may need to be adjusted during the course of treatment to account for changes in the residual motion.

The beam-to-beam and day-to-day variations indicate that, for some patients, residual motion can have pronounced changes during a course of treatment. This will be most problematic in treatments consisting of only a few fractions, where an anomalously large residual motion during one beam/day will have a greater overall effect than during a longer treatment. It would be best to use some method of online verification or real-time marker/tumour tracking in order to confidently gate treatment.

Acknowledgments

This work was partially supported by grants from Varian Medical Systems and the Whitaker Foundation. The authors would like to acknowledge Dr Greg Sharp and Dr Toni Neicu of

Massachusetts General Hospital, Dr Takeshi Nishioka of Hokkaido University and Ms Kristin Canavan for their help with this work.

References

Balter J M *et al* 1996 Uncertainties in CT-based radiation therapy treatment planning associated with patient breathing *Int. J. Radiat. Oncol. Biol. Phys.* **36** 167–74

Barnes E A *et al* 2001 Dosimetric evaluation of lung tumor immobilization using breath hold at deep inspiration *Int. J. Radiat. Oncol. Biol. Phys.* **50** 1091–8

Berbeco R *et al* 2004 Tumor tracking in the absence of radiopaque markers. in *XIVth ICCR. (Seoul, South Korea)*

Bryan P J *et al* 1984 Respiration movement of the pancreas: An ultrasonic study *J. Ultrasound Med.* **3** 317–320

Davies S C *et al* 1994 Ultrasound quantitation of respiratory organ motion in the upper abdomen *Br. J. Radiol.* **67** 1096–102

Ekberg L *et al* 1998 What margins should be added to the clinical target volume in radiotherapy treatment planning for lung cancer? *Radiother. Oncol.* **48** 71–7

Harada T *et al* 2002 Real-time tumor-tracking radiation therapy for lung carcinoma by the aid of insertion of a gold marker using bronchofiberscopy *Cancer* **95** 1720–7

Keall P J *et al* 2001 Motion adaptive x-ray therapy: a feasibility study *Phys. Med. Biol.* **46** 1–10

Kini V R *et al* 2003 Patient training in respiratory-gated radiotherapy *Med. Dosim.* **28** 7–11

Kubo H D and Hill B C 1996 Respiration gated radiotherapy treatment: a technical study *Phys. Med. Biol.* **41** 83–91

Kubo H D and Wang L 2002 Introduction of audio gating to further reduce organ motion in breathing synchronized radiotherapy *Med. Phys.* **29** 50

Langen K M and Jones D T 2001 Organ motion and its management *Int. J. Radiat. Oncol. Biol. Phys.* **50** 265–78

Mageras G S and Yorke E 2004 Deep inspiration breath hold and respiratory gating strategies for reducing organ motion in radiation treatment *Semin. Radiat. Oncol.* **14** 65–75

Mageras G S *et al* 2001 Fluoroscopic evaluation of diaphragmatic motion reduction with a respiratory gated radiotherapy system *J. Appl. Clin. Med. Phys.* **2** 191–200

Maruhashi A, Tsuji H and Sato M 1992 Development of a moving target aiming system using an ultrasound imaging unit *Nippon Igaku Hoshasen Gakkai Zasshi* **52** 1001–6

Minohara S *et al* 2000 Respiratory gated irradiation system for heavy-ion radiotherapy *Int. J. Radiat. Oncol. Biol. Phys.* **47** 1097–103

Neicu T *et al* 2003 Synchronized moving aperture radiation therapy (SMART): average tumour trajectory for lung patients *Phys. Med. Biol.* **48** 587–98

Neicu T *et al* 2004 Patient breathing coaching using the real position management system *Med. Phys.* **31** 1907

Ohara K *et al* 1989 Irradiation synchronized with respiration gate *Int. J. Radiat. Oncol. Biol. Phys.* **17** 853–7

Ross C S *et al* 1990 Analysis of movement of intrathoracic neoplasms using ultrafast computerized tomography *Int. J. Radiat. Oncol. Biol. Phys.* **18** 671–7

Schweikard A *et al* 2000 Robotic motion compensation for respiratory movement during radiosurgery *Comput. Aided Surg.* **5** 263–77

Shimizu S *et al* 1999 Three-dimensional movement of a liver tumor detected by high-speed magnetic resonance imaging *Radiother. Oncol.* **50** 367–70

Shirato H *et al* 2000a Physical aspects of a real-time tumor-tracking system for gated radiotherapy *Int. J. Radiat. Oncol. Biol. Phys.* **48** 1187–95

Shirato H *et al* 2000 Four-dimensional treatment planning and fluoroscopic real-time tumor tracking radiotherapy for moving tumor *Int. J. Radiat. Oncol. Biol. Phys.* **48** 42

Shirato H *et al* 2003 Feasibility of insertion/implantation of 2.0-mm-diameter gold internal fiducial markers for precise setup and real-time tumor tracking in radiotherapy *Int. J. Radiat. Oncol. Biol. Phys.* **56** 240–7

Suramo I, Paivansalo M and Myllyla V 1984 Cranio-caudal movements of the liver, pancreas and kidneys in respiration *Acta Radiol. Diagn.* **25** 129–31

Weiss P H, Baker J M and Potchen E J 1972 Assessment of hepatic respiratory excursion *J. Nucl. Med.* **13** 758–9

Wong J W *et al* 1999 The use of active breathing control (ABC) to reduce margin for breathing motion *Int. J. Radiat. Oncol. Biol. Phys.* **44** 911–9

Zhang T *et al* 2003 Application of the spirometer in respiratory gated radiotherapy *Med. Phys.* **30** 3165–71

ELSEVIER

Int. J. Radiation Oncology Biol. Phys., Vol. 64, No. 4, pp. 1229–1236, 2006

0360-3016/06/$–see front matter

doi:10.1016/j.ijrobp.2005.11.016

PHYSICS CONTRIBUTION

SPEED AND AMPLITUDE OF LUNG TUMOR MOTION PRECISELY DETECTED IN FOUR-DIMENSIONAL SETUP AND IN REAL-TIME TUMOR-TRACKING RADIOTHERAPY

HIROKI SHIRATO, M.D.,* KEISHIRO SUZUKI, M.D.,* GREGORY C. SHARP, PH.D.,†
KATSUHISA FUJITA, R.T.,* RIKIYA ONIMARU, M.D.,* MASAHARU FUJINO, M.D.,* NORIO KATO, M.D.,*
YASUHIRO OSAKA, M.D.,* RUMIKO KINOSHITA, M.D.,* HIROSHI TAGUCHI, M.D.,*
SHUNSUKE ONODERA, M.D.,* AND KAZUO MIYASAKA, M.D.*

*Department of Radiology, Hokkaido University School of Medicine, Sapporo, Japan; †Department of Radiation Oncology, Massachusetts General Hospital, Harvard Medical School, Boston, MA

Background: To reduce the uncertainty of registration for lung tumors, we have developed a four-dimensional (4D) setup system using a real-time tumor-tracking radiotherapy system.
Methods and Materials: During treatment planning and daily setup in the treatment room, the trajectory of the internal fiducial marker was recorded for 1 to 2 min at the rate of 30 times per second by the real-time tumor-tracking radiotherapy system. To maximize gating efficiency, the patient's position on the treatment couch was adjusted using the 4D setup system with fine on-line remote control of the treatment couch.
Results: The trajectory of the marker detected in the 4D setup system was well visualized and used for daily setup. Various degrees of interfractional and intrafractional changes in the absolute amplitude and speed of the internal marker were detected. Readjustments were necessary during each treatment session, prompted by baseline shifting of the tumor position.
Conclusion: The 4D setup system was shown to be useful for reducing the uncertainty of tumor motion and for increasing the efficiency of gated irradiation. Considering the interfractional and intrafractional changes in speed and amplitude detected in this study, intercepting radiotherapy is the safe and cost-effective method for 4D radiotherapy using real-time tracking technology. © **2006 Elsevier Inc.**

Four-dimensional radiotherapy, Setup, Real-time tracking, Four-dimensional setup.

INTRODUCTION

Four-dimensional (4D) radiotherapy, a concept to increase the accuracy of localization in space as well as in time by accounting for spatiotemporal changes in the anatomy during radiotherapy, has been receiving more and more attention (1). Four-dimensional treatment planning is increasingly used to reduce the uncertainty resulting from organ motion of computed tomography (CT) (1–3). Second, a therapeutic beam is delivered to the moving tumor by real-time tumor-tracking technology in which a gated beam intercepts the tumor trajectory (4) or in which the tumor position is pursued dynamically (5). Third, verification of the tumor position during irradiation is required for quality assurance (6). Each step in 4D radiotherapy (4DRT) is quite important. One of the most important steps is the accurate registration of the tumor position at the same phase of internal tumor motion as in the treatment planning. Without this, we will miss the tumor in 4DRT.

To our knowledge, no 4D setup method—that is, a method for setting up tumors in motion at the right time and with the right coordinates—has been reported. We have developed a 4D setup system using a fluoroscopic real-time tumor-tracking radiotherapy (RTRT) system (1, 4). In this paper, we describe our approach to performing 4D setup using the RTRT system. We describe also what we have found about interfractional and intrafractional changes in the amplitude and speed of internal tumor motion using the 4D setup system.

METHODS AND MATERIALS

Four-dimensional setup

The RTRT system has been already described in detail (1, 4). In brief, three 1.5-mm fiducial markers are implanted near a lung tumor through bronchial fiberscopy. Two sets of fluoroscopy in the treatment room are used to detect the three-dimensional (3D) coordinates of each internal fiducial marker. The distances be-

Reprint requests to: Hiroki Shirato, Department of Radiology, Hokkaido University School of Medicine, North-15 West-7, Sapporo 060-8636, Japan. Tel: (+81) 11-706-7876; Fax: (+81) 11-706-5975; E-mail: hshirato@radi.med.hokudai.ac.jp

Received Aug 5, 2005, and in revised form Nov 8, 2005. Accepted for publication Nov 17, 2005.